

Strain-Mediated Interlayer Coupling Effects on the Excitonic Behaviors in an Epitaxially Grown MoS₂/WS₂ van der Waals Heterobilayer

Sangyeon Pak,[†] Juwon Lee,[†] Young-Woo Lee,[†] A-Rang Jang,^{†,‡} Seongjoon Ahn,[‡] Kyung Yeol Ma,[‡] Yuljae Cho,[†] John Hong,[†] Sanghyo Lee,[†] Hu Young Jeong,[§] Hyunsik Im,^{||} Hyeon Suk Shin,[‡] Stephen M. Morris,[†] SeungNam Cha,^{*,†} Jung Inn Sohn,^{*,†} and Jong Min Kim[⊥]

[†]Department of Engineering Science, University of Oxford, Parks Road, Oxford OX1 3PJ, United Kingdom

[‡]Department of Chemistry and Department of Energy Engineering, Low-Dimensional Carbon Materials Center, Ulsan National Institute of Science and Technology (UNIST), UNIST-gil 50, Ulsan 44919, Republic of Korea

[§]UNIST Central Research Facilities (UCRF), Ulsan National Institute of Science and Technology (UNIST), 50 UNIST-gil, Ulsan 44919, Republic of Korea

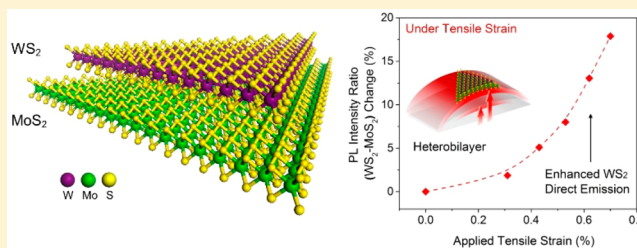
^{||}Division of Physics and Semiconductor Science, Dongguk University, Seoul 100-715, Republic of Korea

[⊥]Department of Engineering, University of Cambridge, 9 JJ Thomson Avenue, Cambridge CB3 0FA, United Kingdom

Supporting Information

ABSTRACT: van der Waals heterostructures composed of two different monolayer crystals have recently attracted attention as a powerful and versatile platform for studying fundamental physics, as well as having great potential in future functional devices because of the diversity in the band alignments and the unique interlayer coupling that occurs at the heterojunction interface. However, despite these attractive features, a fundamental understanding of the underlying physics accounting for the effect of interlayer coupling on the interactions between electrons, photons, and phonons in the stacked heterobilayer is still lacking. Here, we demonstrate a detailed analysis of the strain-dependent excitonic behavior of an epitaxially grown MoS₂/WS₂ vertical heterostructure under uniaxial tensile and compressive strain that enables the interlayer interactions to be modulated along with the electronic band structure. We find that the strain-modulated interlayer coupling directly affects the characteristic combined vibrational and excitonic properties of each monolayer in the heterobilayer. It is further revealed that the relative photoluminescence intensity ratio of WS₂ to MoS₂ in our heterobilayer increases monotonically with tensile strain and decreases with compressive strain. We attribute the strain-dependent emission behavior of the heterobilayer to the modulation of the band structure for each monolayer, which is dictated by the alterations in the band gap transitions. These findings present an important pathway toward designing heterostructures and flexible devices.

KEYWORDS: van der Waals heterostructures, MoS₂/WS₂, strain engineering, interlayer interactions, band gap transition



Semiconductor heterostructures with different electronic band gap energies and electron affinities have long been of considerable interest for both fundamental condensed matter physics and potential applications in modern electronics and optoelectronics as well as energy conversion systems.^{1–3} Recently, notable progress in the field of heterostructures has been made resulting in the development of high performance, high speed, and high power devices through improvements in the experimental technique and the theoretical understanding.^{4–8} Moreover, to open up new avenues beyond the limit of conventional bulk semiconductor structures, many efforts have been focused on developing new semiconducting nanomaterials as well as understanding the various underlying physical phenomena that occur at the heterojunction interface. These in turn allow for the creation of new device and structure

concepts with unique functionality, which is particularly relevant to the development of next-generation flexible and wearable device applications.^{1,9–12}

In this regard, two-dimensional (2D) atomic monolayers including graphene,^{11,13} hexagonal boron nitride (h-BN),^{14–16} and transition metal dichalcogenides (TMDCs)^{17,18} have attracted notable attention as they can be assembled vertically so that distinct 2D monolayers can be integrated into van der Waals heterostructures with structurally abrupt and chemically clean interfaces.¹⁹ To date, these monolayers have been stacked in such a way so as to form variety of 2D heterostructures with

Received: June 14, 2017

Revised: August 17, 2017

Published: August 23, 2017

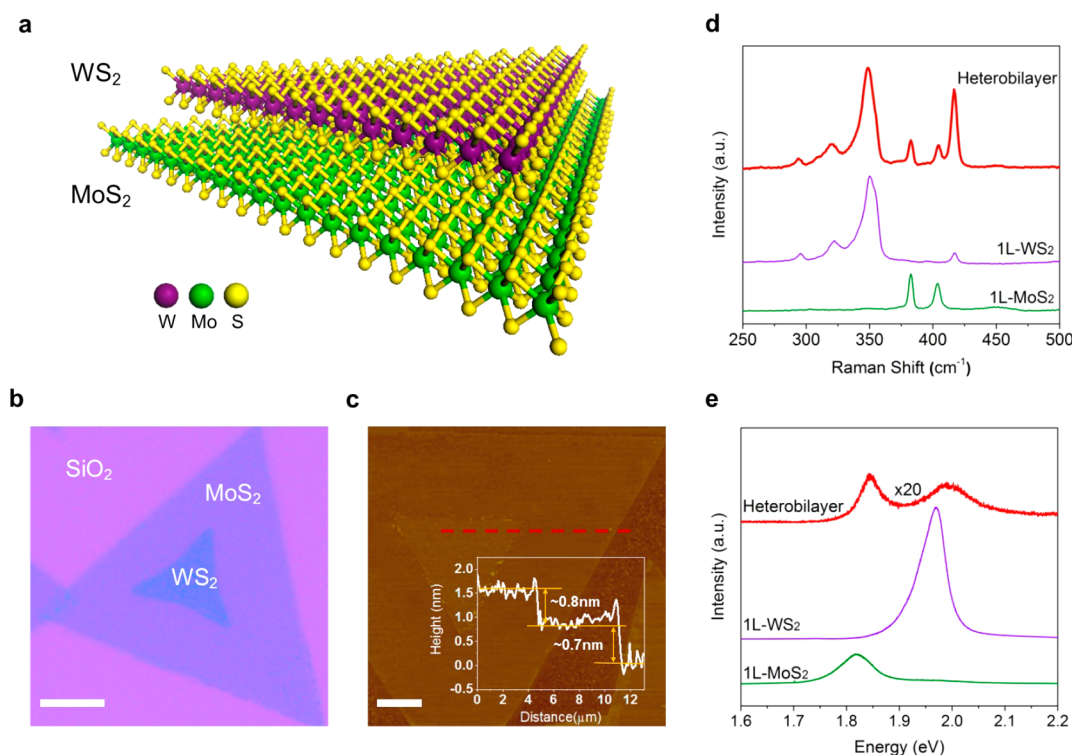


Figure 1. Synthesis and characterization of a MoS₂/WS₂ heterobilayer. (a) A schematic representation of a CVD grown MoS₂/WS₂ heterobilayer with WS₂ grown on top of MoS₂. (b) An optical image of the CVD grown heterobilayer on a 300 nm SiO₂ substrate. Note that WS₂ is grown on top of MoS₂, which can be distinguished from the distinct optical contrast in the colors for the different layers. Scale bar: 10 μ m. (c) An AFM topography image of the CVD grown heterobilayer. The thickness of monolayer WS₂ and MoS₂ is extracted to be 0.8 and 0.7 nm, respectively, from the height profile (inset) at the vertical step edge of a MoS₂/WS₂ heterobilayer and MoS₂/SiO₂, which confirms the formation of the MoS₂/WS₂ heterobilayer. Scale bar: 3 μ m. (d) Raman spectra of the heterobilayer (red curve) and individual monolayers of MoS₂ and WS₂. For a MoS₂/WS₂ heterobilayer, the Raman characteristic peaks of each monolayer appear to coexist. (e) PL spectra taken from the heterobilayer (red curve). The PL intensity of the heterobilayer is noticeably decreased compared to that recorded for individual monolayers of MoS₂ and WS₂.

unique heterojunction configurations such as MoS₂/WS₂,^{20–24} MoS₂/WSe₂,^{25–28} MoSe₂/WSe₂,^{29–31} WS₂/WSe₂,³² and graphene/MoS₂.³³ In each case, the design is driven by considering the alignments of the energy bands and the charge transport model so that it is suitable for a range of optoelectronic device applications. In particular, it has been demonstrated that heterobilayers of different 2D materials can preserve the fundamental properties of each individual monolayer; this means that excitonic behavior and electronic band structure of each monolayer can coexist in the stacked heterobilayer system, leading to unique and distinct physics and device performance compared to 2D homobilayers.^{20,34,35}

It is well established from both theoretical^{36,37} and experimental^{38–40} studies that strain can be utilized as an effective strategy for engineering the electronic band structure and modulating the excitonic behavior in 2D semiconducting materials; this is because the transition metal 4d sulfur 3p orbital interactions and hybridizations are easily affected by any strain that is imparted on the material.^{36,38–45} It is thus expected that strain engineering provides a means for addressing the scientific challenges associated with designing and tailoring the unique and attractive features of van der Waals coupled heterostructures, enabling the realization of novel electronic and optoelectronic devices. However, despite the high importance of understanding the strain-induced modulation of 2D heterobilayers for future flexible heterostructure devices, most studies on strain effects have focused only on TMDCs monolayers (e.g., MoS₂,^{39,45} WS₂,⁴⁶ MoSe₂,³⁸ and

WSe₂⁴⁰). Further, there are no detailed accounts describing the strain-dependent evolution of the excitonic behavior in a heterobilayer system and the relationship between the strain-induced electronic band structure transitions for two different monolayers where each individual monolayer can be differently affected by strain.

Herein, we investigate the uniaxial strain-mediated evolution of the phonon energy and exciton emission in a high quality MoS₂/WS₂ heterostructure with an epitaxial interface using Raman and photoluminescence (PL) spectroscopy. For this, we employ a one-step epitaxial growth method to obtain a clean, structurally abrupt junction so as to eliminate any unwanted effects²¹ such as contamination, defects, and rotational misalignments, which are unavoidably introduced into the interface in heterostructure samples that have been fabricated using a transfer process. We demonstrate a clear relationship between interlayer interactions and excitonic behavior, which is closely related to the transition of the energy band structure of the MoS₂/WS₂ heterobilayer, and that show opposing behavior under uniaxial tensile and compressive strain. Moreover, we observe directly that the combined vibrational and emissive properties of two different monolayers in the heterostructure are modulated separately by the strain while retaining the characteristics of each monolayer.

A vertical MoS₂/WS₂ heterobilayer was grown directly on a 300 nm SiO₂/Si substrate via the epitaxial growth of WS₂ on top of the MoS₂ monolayer using our unique one-step CVD growth method (see Supporting Information). Figure 1a,b

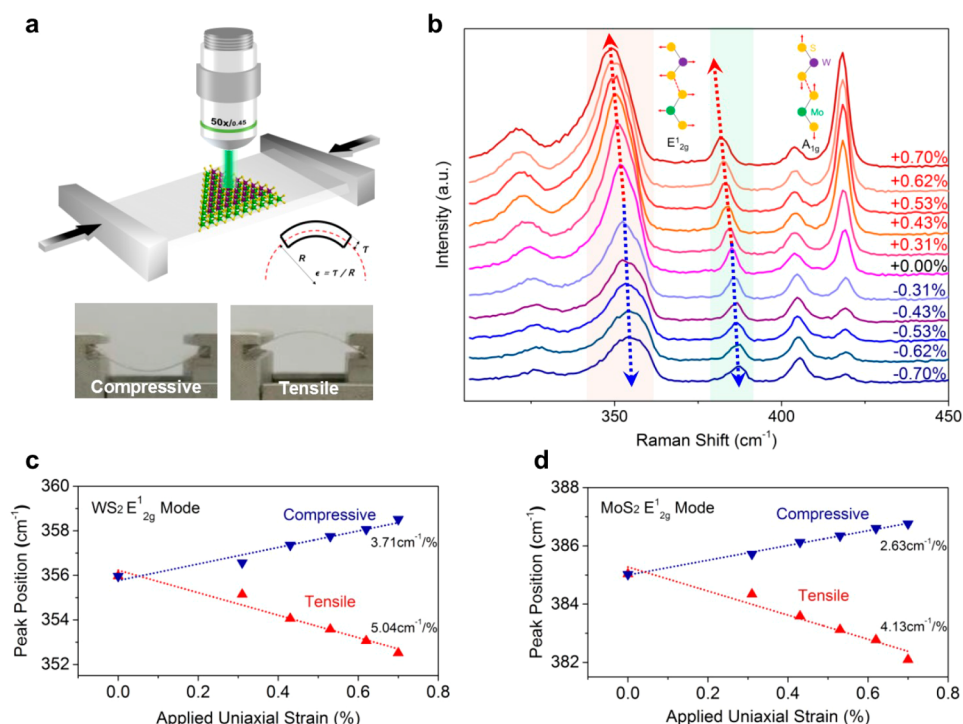


Figure 2. Characteristic phonon vibrational modes of the MoS₂/WS₂ heterobilayer under tensile and compressive strain. (a) A schematic of our bending system used to strain the heterobilayer and measure the vibrational phonon modes. (b) Evolution of the Raman spectra as the heterobilayer is strained from 0% to +0.70% (toward red, tensile) and −0.70% (toward blue, compressive). The change in the Raman in-plane E_{12g} phonon modes of WS₂ (c) and MoS₂ (d) in the heterobilayer under uniaxial tensile (red) and compressive (blue) strain.

shows a schematic and an optical image of the as-grown triangular MoS₂/WS₂ heterostructure, respectively, which is formed vertically.²² The heterobilayer feature consisting of morphologically distinct monolayers was clearly identified by comparing the optical color contrast (Figure 1b) and AFM image (Figure 1c), showing that WS₂ was grown on top of the MoS₂ monolayer with AA-stacking (3R phase) as also was confirmed in Figure S1. It is worth mentioning that the directly grown MoS₂/WS₂ heterostructures with the epitaxial interface can result in strong coupling between the monolayers.²² This highlights the merit of our heterostructure samples over the mechanically transferred samples, which enables a detailed understanding of the interlayer coupling in the van der Waals heterobilayer by ruling out any contamination effects and/or rotational misalignment effects.

Raman and PL spectroscopy were performed to investigate the structural and optical characteristics of the as-grown heterostructure. For a comparison, Raman spectra of individual monolayers and heterobilayer samples were obtained together using a 532 nm laser with a spot size of ~1 μm as shown in Figure 1d. As expected, for the monolayer MoS₂, two typical characteristic peaks were observed at 382.8 and 402.7 cm⁻¹, in accordance with the in-plane vibrational mode (E_{12g} mode) and the out-of-plane vibrational mode (A_{1g} mode), respectively, while for the monolayer WS₂, two Raman peaks located at 349 and 417 cm⁻¹ were observed, which can be assigned to the overlapping 2LA (longitudinal acoustic mode at the M point) and E_{12g} modes and the A_{1g} mode, respectively. Unlike MoS₂, Lorentzian fitting to the peaks of the Raman spectra for monolayer WS₂ reveals that there are many second-order peaks such as the 2LA mode around 350 cm⁻¹ that are much stronger than the first-order peak⁴⁷ (Figure S2). The appearance of the peaks might be associated with the 532 nm laser wavelength

employed in our work because such an excitation laser source is in resonance with the B exciton peak of the WS₂.^{47–49}

The Raman spectra of the heterobilayer were found to comprise all the characteristic peaks of both the individual MoS₂ and WS₂ monolayer, implying the formation of the MoS₂/WS₂ heterobilayer. Interestingly, it can be seen that the intensity of the WS₂ A_{1g} peak in the heterostructure is largely enhanced. It is reported that the A_{1g} peak intensity of WS₂ increases with an increase in the numbers of layers because the intensity of the WS₂ A_{1g} mode is very sensitive to the layer thickness.⁴⁷ Thus, we suggest that this enhancement of the WS₂ A_{1g} peak intensity indicates the formation of the heterobilayer, which is consistent with AFM results shown in Figure 1c. The Raman intensity mapping images of the MoS₂ A_{1g} mode peak and the WS₂ A_{1g} mode peak further demonstrate that the vertically stacked heterostructure consists of monolayer MoS₂ and WS₂ as shown in Figure S3. Similar to the Raman results presented in Figure 1d, the PL spectra (Figure 1e) obtained from the MoS₂ and WS₂ monolayers show strong emission peaks at their characteristic direct excitonic energies of 1.824 eV (λ = 680 nm) and 1.968 eV (λ = 630 nm), respectively. Also, it is observed that the heterobilayer exhibits two emission peaks due to the coupling between the individual monolayers in the heterostructure. In contrast to the monolayers, however, there is a significant reduction in the PL intensity. The reduced PL intensity can be attributed to the interlayer exciton dissociation (the separation of excited electron and hole pairs) associated with the type II heterojunction.^{6,50}

To gain fundamental insight into the nature of the interlayer coupling in vertically stacked TMDC van der Waals heterostructures, we have investigated the strain-dependent evolution of the Raman spectra of the MoS₂/WS₂ heterobilayer under both uniaxial tensile and compressive strain as shown in

Figure 2a. For this, the CVD-grown heterobilayer sample was first transferred onto the flexible PET substrate so that the strain-induced interlayer interaction effects, which can alter the vibrations of the phonon modes in the heterostructure, could be observed by applying a uniaxial strain using our bespoke bending experimental apparatus. **Figure 2b** shows the strain dependence of the Raman spectra obtained from the CVD-grown heterobilayer sample transferred onto the PET substrate (**Figure S4**) under tensile (toward red color) and compressive (toward blue color) strain. The applied strain was calculated using $\varepsilon = \tau/R$, where 2τ is the thickness of the PET substrate ($125\ \mu\text{m}$) and R is the radius of curvature. Interestingly, we found that the in-plane E_{2g}^1 modes of the heterobilayer show strong strain-dependent phonon shifts, while the out-of-plane A_{1g} modes of the heterobilayer show negligible shifts under applied uniaxial strain.

To further elucidate the strain-induced modulation of the phonon vibrational mode, the change in the peak positions of the E_{2g}^1 modes were plotted as a function of strain (**Figure 2c,d**). It can be seen that for an applied strain in the range of 0–0.7%, the E_{2g}^1 peak in the heterobilayer was found to shift linearly with strain and from this the linear shift rates were determined to be -4.13 and $2.63\ \text{cm}^{-1}$ for tensile and compressive strain, respectively in MoS_2 and -5.04 and $3.71\ \text{cm}^{-1}$ for tensile and compressive strain in WS_2 , respectively. It was also observed that the frequency of the E_{2g}^1 modes was more strongly affected under tensile strain than compressive strain. It is expected that the bond length of $\text{Mo(W)}\text{-S}$ increases while interlayer S–S distance decreases under tensile strain, and the opposite trend is expected under compressive strain, which could explain a phonon frequency softening (stiffening) in the heterobilayer as a result of an increase (decrease) in the lattice constant under tensile (compressive) strain.^{40,45} In other words, the decrease in the interlayer distance under tensile strain induces a stronger interlayer interaction between the layers compared to that observed for compressive strain, thus resulting in a significantly enhanced interlayer coupling between the MoS_2 and WS_2 layers. This enhanced coupling induces more strong dependence of the E_{2g}^1 modes on tensile strain. Also, we note that the Raman intensity of phonon modes in WS_2 was found to be affected by applied strain. It was previously reported that the Raman intensity of 2D TMDCs is modulated when excitation laser energy is in resonance with excited states of TMDC materials.^{47,51,52} Thus, we suggest that our observation of intensity changes in the A_{1g} and 2LA phonon modes might be related to the interaction between the excitation laser energy and B exciton energy of monolayer WS_2 , which is affected by strain.

To understand in detail how the strain-modulated interlayer interaction affects the excitonic behavior in the heterobilayered structure and how each monolayer plays a role in determining the resultant optical properties, we have characterized the evolution of the electronic band structure of the heterobilayer using in situ strain PL measurements. **Figure 3a** shows the emergence of the strain-dependent coupled PL spectra recorded as a function of both tensile and compressive strain applied to the MoS_2/WS_2 heterobilayer. It can be seen that both the coupled PL peaks corresponding to each monolayer are modulated separately by the strain while retaining the characteristic coupled emission feature. Moreover, we have observed linear red shifts ($63.4\ \text{meV}/\%$ for MoS_2 and $68.4\ \text{meV}/\%$ for WS_2) and linear blue shifts ($36.3\ \text{meV}/\%$ for MoS_2 and $23.9\ \text{meV}/\%$ for WS_2) of the PL peaks with increasing

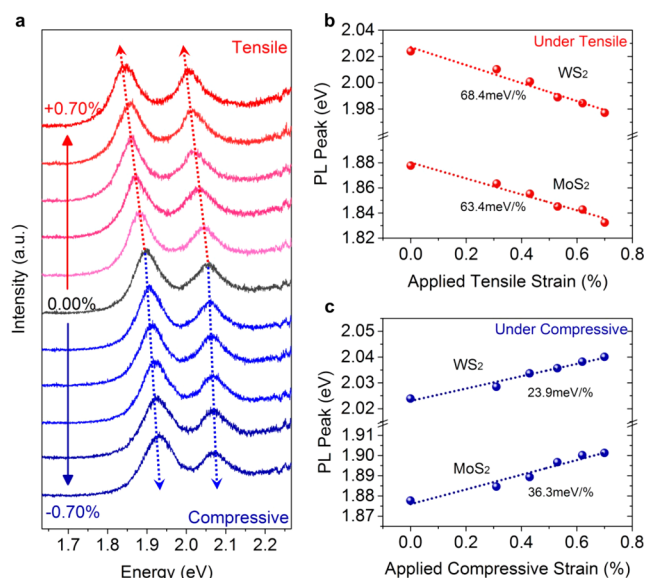


Figure 3. Strain-dependent emission properties of the MoS_2/WS_2 heterobilayer. (a) Evolution of the PL spectra as the heterobilayer is strained from 0% (black) to +0.7% (toward red, tensile) and -0.7% (toward blue, compressive). Strain-dependent PL peak position of coupled MoS_2 and WS_2 in the heterobilayer under uniaxial (b) tensile and (c) compressive strain.

tensile and compressive strain, respectively, (**Figures 3b,c**). In principle, the PL shift can be considered to be an indicator of how the electronic band structure is altered by the application of strain. The trends observed for the shifts in the PL peak and the sensitivity of the spectra to the strain applied to our heterobilayer sample are consistent with previous theoretical calculations^{36,37} and experiments^{39,46} based on strained monolayer TMDCs, which have observed a reduction or increase in the electronic band gap. We therefore believe that the overall optical characteristics of the MoS_2/WS_2 heterobilayer are strongly dependent on the evolution of the electronic band structure in each monolayer.

In order to further understand the relationship between the strain-induced electronic band structure modulation and the corresponding exciton transition behavior in the heterobilayer, we have also analyzed and compared the change in the PL spectra of individual MoS_2 and WS_2 monolayers with those of a heterobilayer induced by strain (**Figures S5–7** and **Figure 3**). We note that although the differences in the magnitude of the shift rates between the monolayer and the heterobilayer were not significantly noticeable under uniaxial compressive strain, the tensile strain was found to noticeably affect the emission peaks in the heterobilayer compared to that of the monolayers of MoS_2 and WS_2 (the shift rates for the heterobilayer were found to increase by more than 20% under tensile strain compared to that under compressive strain as shown in **Figure S6**). This indicates that the interlayer interaction between the monolayers in the heterobilayer has a stronger impact on the electronic band structure under applied tensile strain, showing similar behavior with the in-plane E_{2g}^1 peak in the Raman spectra.

Further, to clearly elucidate the mechanism underpinning the exciton transitions that are associated with the strain modulated heteroband structure, we have studied the PL intensity as a function of strain, which has been extracted from **Figure 3a**. Interestingly, the relative intensity ratio of WS_2 to MoS_2 in the

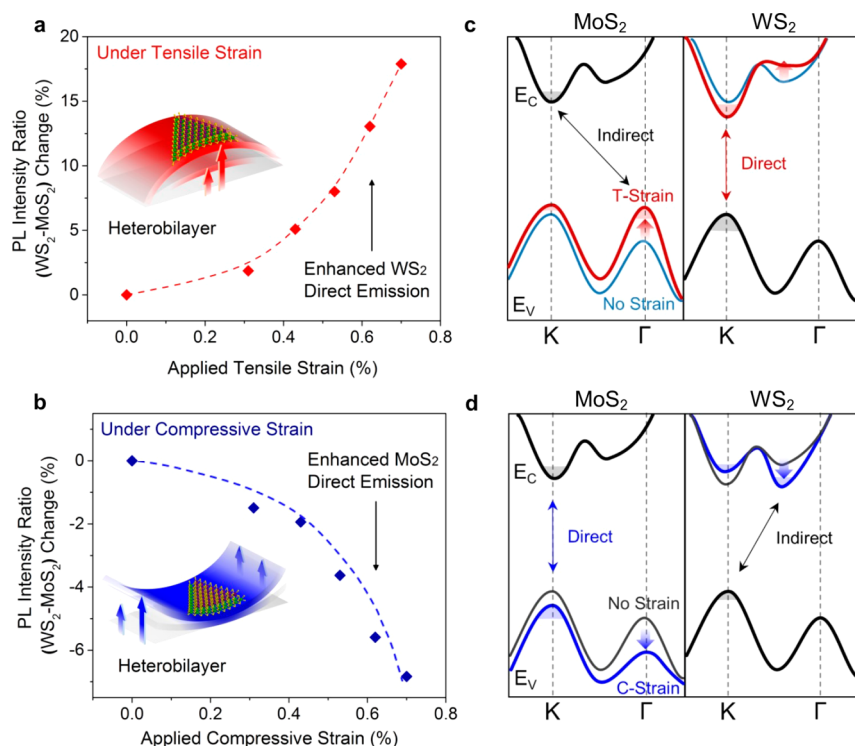


Figure 4. Variation in the PL intensity in the heterobilayer and a schematic representation of the band structure under strain. The dependence of the WS_2 to MoS_2 PL intensity ratio in the heterobilayer under (a) tensile and (b) compressive strains. The intensity ratio is monotonically increased and decreased under tensile and compressive strain, respectively. A schematic representation showing the contrasting trends of the evolution of electronic band structure in monolayers of MoS_2 and WS_2 under (c) tensile (red) and (d) compressive (blue) strain. “direct” and “indirect” represent the direct semiconducting characteristic and direct to indirect transition, respectively.

heterobilayer was found to monotonically increase (up to 20%) under tensile strain, while under compressive strain the relative intensity was found to decrease (down to 7%) as shown in Figures 4a,b. Here, we note that the monolayer of MoS_2 (Figure S7a) and that of WS_2 (Figure S7b) show a contrasting trend in the change in PL intensity under tensile and compressive strains, which is consistent with previously reported theoretical calculations and experimental demonstrations of the strain-dependent band structure evolution of monolayer MoS_2 and WS_2 . When a tensile strain is applied, the PL intensity is decreased for MoS_2 and increased for WS_2 . In contrast, the PL intensity is increased for MoS_2 and decreased for WS_2 when a compressive strain is applied. Such behavior originates from the transition between a direct and indirect band gap (and vice versa), which is different in strained monolayers of MoS_2 and WS_2 and is discussed in more detail in the next section. Thus, even though the origin of the changes in the PL intensity in the heterobilayer is still unclear, we attribute the strain-dependent emission properties to a combined modulation of the band structures for each monolayer within the heterobilayer.

It should be noted that for single monolayer crystals, MoS_2 undergoes a direct-to-indirect transition while for WS_2 the direct semiconducting characteristic is reinforced under tensile strain, and vice versa under compressive strain,^{36,37,39,40} revealing the contrasting evolution of the band structure as depicted in Figure 4c,d. That is, as confirmed by theoretical and experimental studies,^{36,39} for a monolayer of MoS_2 (Figure 4 panel c left and panel d left), the transition in the band gap is predominantly governed by a change in the energy of the local valence band (VB) maxima where the indirect VB maxima at

the Γ -point shifts up (down) with tensile (compressive) strain more rapidly than the direct VB maxima at the K-point. On the contrary, for a monolayer of WS_2 , however, it is predicted theoretically³⁷ that under tensile strain the direct semiconducting characteristics are reinforced (Figure 4c right) and that it undergoes a direct-to-indirect transition under compressive strain (Figure 4d right). This is because the evolution of the band gap is driven by the conduction band (CB) minima of WS_2 , which is changed as result of opposite shifts in the energy at the K and K- Γ points. The interpretation of these trends is consistent with our experimental and simulation results (Figures S7 and 8), showing the different dependence of the PL intensities of monolayers of MoS_2 and WS_2 on the applied strain.

In this regard, it is anticipated that the heterobilayer retains the direct optical band gap characteristic regardless of any strain environment by complementing the PL properties of monolayers of MoS_2 and WS_2 , which exhibit markedly opposing strain dependencies. In other words, the enhancement of the PL intensity for WS_2 is dominant through the reinforcement of its direct band gap characteristic with tensile strain, whereas under compressive strain the direct semiconducting nature of MoS_2 is also strengthened relatively, leading to an enhancement in the PL intensity of MoS_2 in the heterobilayer. As a result, it is believed that the relative increase (decrease) in the PL intensity ratio of WS_2 to MoS_2 in the heterostructure is attributed to an enhancement (weakening) in the PL intensity of WS_2 along with a weakening (enhancement) of the PL intensity of MoS_2 under tensile (compressive) strain. These findings indicate that the emission properties of the heterobilayer are different from those of the homobilayer and

complement one another through the crossovers between a direct and indirect band gap in monolayers of MoS₂ and WS₂.

In conclusion, we have investigated the strain-dependent phonon modulation, emission properties, and the complementary changes in the PL intensity of an epitaxial-grown MoS₂/WS₂ heterobilayer when subjected to tensile and compressive strains. Interlayer interactions are shown to strongly affect the band structure of the heterobilayer, which is confirmed by the enhanced shift rates of the in-plane vibrational phonon modes and the PL emission peaks under tensile strain. By carefully examining the strain-dependent changes in the WS₂ to MoS₂ PL intensity ratio of the heterobilayer, we observe that the excitonic behavior is governed by the combined evolution of the band structure of the individual monolayers of MoS₂ and WS₂, which exhibit different dependencies on the strain. These observations strongly support that strain engineering is a versatile tool with which to explore the various fundamental material properties of MoS₂/WS₂ heterostructures as well as in many other combinations of 2D van der Waals materials. We believe that our findings contribute to the understanding of electron, photon, and phonon dynamics in the heterostructures, which is of importance for the development of flexible and transparent (opto)electronics technologies.

■ ASSOCIATED CONTENT

Supporting Information

The Supporting Information is available free of charge on the ACS Publications website at DOI: [10.1021/acs.nanolett.7b02513](https://doi.org/10.1021/acs.nanolett.7b02513).

Detailed description of the sample fabrication and characterization, TEM analysis of the heterobilayer, Raman spectrum of monolayers of MoS₂ and WS₂, Raman intensity mapping of MoS₂/WS₂ heterobilayer, Raman spectrum of transferred MoS₂/WS₂ heterobilayer, optical image of monolayers of MoS₂ and WS₂, strain-dependent photoluminescence peak shifts and intensity changes, DFT calculations of strained MoS₂ and WS₂ (PDF)

■ AUTHOR INFORMATION

Corresponding Authors

*Tel: +44-1865-283034. Fax: +44-1865-273010. E-mail: seungnam.cha@eng.ox.ac.uk.

*Tel: +44-1865-273912. Fax: +44-1865-273010. E-mail: junginn.sohn@eng.ox.ac.uk.

ORCID

Sangyeon Pak: 0000-0003-1765-3043

Yuljae Cho: 0000-0003-2976-0604

John Hong: 0000-0002-1513-8622

Hyeon Suk Shin: 0000-0003-0495-7443

Jung Inn Sohn: 0000-0002-3155-4327

Notes

The authors declare no competing financial interest.

■ ACKNOWLEDGMENTS

This research was supported by the European Research Council under the European Union's Seventh Framework Programme (FP/2007-2013)/Grant Agreements 340538 (Project "UniQDS") and 685758 (Project "1D-NEON"). The authors would also like to thank the financial support from the National

Research Foundation (NRF) of Korea (2015M2A2A6A02045252). In addition, S.M.M. would also like to thank The Royal Society for financial support.

■ REFERENCES

- (1) Geim, A. K.; Grigorieva, I. V. *Nature* **2013**, 499 (7459), 419–425.
- (2) Mori, N.; Ando, T. *Phys. Rev. B: Condens. Matter Mater. Phys.* **1989**, 40 (9), 6175–6188.
- (3) Scharber, M. C.; Mühlbacher, D.; Koppe, M.; Denk, P.; Waldauf, C.; Heeger, A. J.; Brabec, C. J. *Adv. Mater.* **2006**, 18 (6), 789–794.
- (4) Kroemer, H. *Proc. IEEE* **1982**, 70 (1), 13–25.
- (5) Kim, B.-S.; Neo, D. C. J.; Hou, B.; Park, J.; Cho, Y.; Zhang, N.; Hong, J.; Pak, S.; Lee, S.; Sohn, J.; Assender, H. E.; Watt, A. A. R.; Cha, S.; Kim, J. *ACS Appl. Mater. Interfaces* **2016**, 8 (22), 13902–13908.
- (6) Hong, X.; Kim, J.; Shi, S.-F.; Zhang, Y.; Jin, C.; Sun, Y.; Tongay, S.; Wu, J.; Zhang, Y.; Wang, F. *Nat. Nanotechnol.* **2014**, 9, 682–686.
- (7) Mimura, T.; Hiyamizu, S.; Fujii, T.; Nanbu, K. *Jpn. J. Appl. Phys.* **1980**, 19 (5), L225–L227.
- (8) Alferov, Z. I. *Semiconductors* **1998**, 32 (1), 1–14.
- (9) Liu, Y.; Weiss, N. O.; Duan, X.; Cheng, H.-C.; Huang, Y.; Duan, X. *Nat. Rev. Mater.* **2016**, 1, 16042.
- (10) Lee, J.; Pak, S.; Lee, Y. W.; Cho, Y.; Hong, J.; Giraud, P.; Shin, H. S.; Morris, S. M.; Sohn, J. I.; Cha, S.; Kim, J. M. *Nat. Commun.* **2017**, 8, 14734.
- (11) Novoselov, K. S.; Fal'ko, V. I.; Colombo, L.; Gellert, P. R.; Schwab, M. G.; Kim, K. *Nature* **2012**, 490 (7419), 192–200.
- (12) Novoselov, K. S.; Mishchenko, A.; Carvalho, A.; Castro Neto, C. A. H. *Science* **2016**, 353 (6298), aac9439.
- (13) Schwierz, F. *Nat. Nanotechnol.* **2010**, 5 (7), 487–496.
- (14) Jang, A. R.; Hong, S.; Hyun, C.; Yoon, S.; Kim, G.; Jeong, H.; Shin, T.; Park, S. O.; Wong, K.; Kwak, S.; Park, N.; Yu, K.; Choi, E.; Mishchenko, A.; Withers, F.; Novoselov, K. S.; Lim, H.; Shin, H. *Nano Lett.* **2016**, 16 (5), 3360–3366.
- (15) Dean, C. R.; Young, A. F.; Meric, I.; Lee, C.; Wang, L.; Sorgenfrei, S.; Watanabe, K.; Taniguchi, T.; Kim, P.; Shepard, K. L.; Hone, J. *Nat. Nanotechnol.* **2010**, 5, 722–726.
- (16) Kim, G.; Jang, A. R.; Jeong, H.; Lee, Z.; Kang, D.; Shin, H. *Nano Lett.* **2013**, 13 (4), 1834–1839.
- (17) Chhowalla, M.; Shin, H. S.; Eda, G.; Li, L.-J. J.; Loh, K. P.; Zhang, H. *Nat. Chem.* **2013**, 5 (4), 263–275.
- (18) Wang, Q. H.; Kalantar-Zadeh, K.; Kis, A.; Coleman, J. N.; Strano, M. S. *Nat. Nanotechnol.* **2012**, 7 (11), 699–712.
- (19) Duan, X.; Wang, C.; Pan, A.; Yu, R.; Duan, X. *Chem. Soc. Rev.* **2015**, 44 (24), 8859–8876.
- (20) Gong, Y.; Lin, J.; Wang, X.; Shi, G.; Lei, S.; Lin, Z.; Zou, X.; Ye, G.; Vajtai, R.; Yakobson, B. I.; Terrones, H.; Terrones, M.; Tay, B.; Lou, J.; Pantelides, S. T.; Liu, Z.; Zhou, W.; Ajayan, P. M. *Nat. Mater.* **2014**, 13 (12), 1135–1142.
- (21) Xue, Y.; Zhang, Y.; Liu, Y.; Liu, H.; Song, J.; Sophia, J.; Liu, J.; Xu, Z.; Xu, Q.; Wang, Z.; Zheng, J.; Liu, Y.; Li, S.; Bao, Q. *ACS Nano* **2016**, 10 (1), 573–580.
- (22) Zhang, J.; Wang, J.; Chen, P.; Sun, Y.; Wu, S.; Jia, Z.; Lu, X.; Yu, H.; Chen, W.; Zhu, J.; Xie, G.; Yang, R.; Shi, D.; Xu, X.; Xiang, J.; Liu, K.; Zhang, G. *Adv. Mater.* **2016**, 28 (10), 1950–1956.
- (23) Lee, J.; Pak, S.; Giraud, P.; Lee, Y. W.; Cho, Y.; Hong, J.; Jang, A. R.; Chung, H. S.; Hong, W. K.; Jeong, H.; Shin, H.; Occhipinti, L. G.; Morris, S. M.; Cha, S.; Sohn, J.; Kim, J. *Adv. Mater.* **2017**, 1702206.
- (24) Bogaert, K.; Liu, S.; Chesin, J.; Titow, D.; Gradečak, S.; Garaj, S. *Nano Lett.* **2016**, 16 (8), 5129–5134.
- (25) Chiu, M.-H.; Zhang, C.; Shiu, H.-W.; Chuu, C.-P.; Chen, C.-H.; Chang, C.-Y. S.; Chen, C.-H.; Chou, M.-Y.; Shih, C.-K.; Li, L.-J. *Nat. Commun.* **2015**, 6, 7666.
- (26) Fang, H.; Battaglia, C.; Carraro, C.; Nemsak, S.; Ozdol, B.; Kang, J.; Bechtel, H. A.; Desai, S. B.; Kronast, F.; Unal, A. A.; Conti, G.; Conlon, C.; Palsson, G. K.; Martin, M. C.; Minor, A. M.; Fadley, C. S.; Yablonovitch, E.; Maboudian, R.; Javey, A. *Proc. Natl. Acad. Sci. U. S. A.* **2014**, 111 (17), 6198–6202.

- (27) Cheng, R.; Li, D.; Zhou, H.; Wang, C.; Yin, A.; Jiang, S.; Liu, Y.; Chen, Y.; Huang, Y.; Duan, X. *Nano Lett.* **2014**, *14* (10), 5590–5597.
- (28) Li, M.-Y.; Shi, Y.; Cheng, C.-C.; Lu, L.-S.; Lin, Y.-C.; Tang, H.-L.; Tsai, M.-L.; Chu, C.-W.; Wei, K.-H.; He, J.-H.; Chang, W.-H.; Suenaga, K.; Li, L.-J. *Science* **2015**, *349* (6247), 524–528.
- (29) He, Y.; Yang, Y.; Zhang, Z.; Gong, Y.; Zhou, W.; Hu, Z.; Ye, G.; Zhang, X.; Bianco, E.; Lei, S.; Jin, Z.; Zou, X.; Yang, Y.; Zhang, Y.; Xie, E.; Lou, J.; Yakobson, B.; Vajtai, R.; Li, B.; Ajayan, P. *Nano Lett.* **2016**, *16* (5), 3314–3320.
- (30) Rivera, P.; Schaibley, J. R.; Jones, A. M.; Ross, J. S.; Wu, S.; Aivazian, G.; Klement, P.; Seyler, K.; Clark, G.; Ghimire, N. J.; Yan, J.; Mandrus, D. G.; Yao, W.; Xu, X. *Nat. Commun.* **2015**, *6*, 6242.
- (31) Gong, Y.; Lei, S.; Ye, G.; Li, B.; He, Y.; Keyshar, K.; Zhang, X.; Wang, Q.; Lou, J.; Liu, Z.; Vajtai, R.; Zhou, W.; Ajayan, P. M. *Nano Lett.* **2015**, *15* (9), 6135–6141.
- (32) Duan, X.; Wang, C.; Shaw, J. C.; Cheng, R.; Chen, Y.; Li, H.; Wu, X.; Tang, Y.; Zhang, Q.; Pan, A.; Jiang, J.; Yu, R.; Huang, Y.; Duan, X. *Nat. Nanotechnol.* **2014**, *9* (12), 1024–1030.
- (33) Roy, K.; Padmanabhan, M.; Goswami, S.; Sai, P. T.; Ramalingam, G.; Raghavan, S.; Ghosh, A. *Nat. Nanotechnol.* **2013**, *8* (11), 826–830.
- (34) Zhang, X.-Q.; Lin, C.-H.; Tseng, Y.-W.; Huang, K.-H.; Lee, Y.-H. *Nano Lett.* **2015**, *15* (1), 410–415.
- (35) Chen, K.; Wan, X.; Xie, W.; Wen, J.; Kang, Z.; Zeng, X.; Chen, H.; Xu, J. *Adv. Mater.* **2015**, *27* (41), 6431–6437.
- (36) Lu, P.; Wu, X.; Guo, W.; Zeng, X. *Phys. Chem. Chem. Phys.* **2012**, *14* (37), 13035–13040.
- (37) Amin, B.; Kaloni, T. P.; Schwingenschlögl, U. *RSC Adv.* **2014**, *4* (65), 34561–34565.
- (38) Tongay, S.; Zhou, J.; Ataca, C.; Lo, K.; Matthews, T. S.; Li, J.; Grossman, J. C.; Wu, J. *Nano Lett.* **2012**, *12* (11), 5576–5580.
- (39) Conley, H.; Wang, B.; Ziegler, J.; Haglund, R.; Pantelides, S.; Bolotin, K. *Nano Lett.* **2013**, *13* (8), 3626–3630.
- (40) Desai, S. B.; Seol, G.; Kang, J.; Fang, H.; Battaglia, C.; Kapadia, R.; Ager, J. W.; Guo, J.; Javey, A. *Nano Lett.* **2014**, *14* (8), 4592–4597.
- (41) Hui, Y.; Liu, X.; Jie, W.; Chan, N.; Hao, J.; Hsu, Y.-T.; Li, L.-J.; Guo, W.; Lau, S. *ACS Nano* **2013**, *7* (8), 7126–7131.
- (42) Liu, Z.; Amani, M.; Najmaei, S.; Xu, Q.; Zou, X.; Zhou, W.; Yu, T.; Qiu, C.; Birdwell, G. A.; Crowne, F. J.; Vajtai, R.; Yakobson, B. I.; Xia, Z.; Dubey, M.; Ajayan, P. M.; Lou, J. *Nat. Commun.* **2014**, *5*, 5246.
- (43) Lloyd, D.; Liu, X.; Christopher, J. W.; Cantley, L.; Wadehra, A.; Kim, B. L.; Goldberg, B. B.; Swan, A. K.; Bunch, S. J. *Nano Lett.* **2016**, *16* (9), 5836–5841.
- (44) Steinhoff, A.; Kim, J. H.; Jahnke, F.; Rösner, M.; Kim, D. S.; Lee, C.; Han, G. H.; Jeong, Wehling, T. O.; Gies, C. *Nano Lett.* **2015**, *15* (10), 6841–6847.
- (45) He, K.; Poole, C.; Mak, K.; Shan, J. *Nano Lett.* **2013**, *13* (6), 2931–2936.
- (46) Wang, Y.; Cong, C.; Yang, W.; Shang, J.; Peimyoo, N.; Chen, Y.; Kang, J.; Wang, J.; Huang, W.; Yu, T. *Nano Res.* **2015**, *8* (8), 2562–2572.
- (47) Berkdemir, A.; Gutiérrez, H. R.; Botello-Méndez, A. R.; Perea-López, N.; Elías, A.; Chia, C.-L.; Wang, B.; Crespi, V. H.; López-Urias, F.; Charlier, J.-C.; Terrones, H.; Terrones, M. *Sci. Rep.* **2013**, *3*, 1755.
- (48) Zhao, W.; Ghorannevis, Z.; Amara, K.; Pang, J.; Toh, M.; Zhang, X.; Kloc, C.; Tan, P.; Eda, G. *Nanoscale* **2013**, *5* (20), 9677–9683.
- (49) Wang, F.; Kinloch, I. A.; Wolverson, D.; Tenne, R.; Zak, A.; O’Connell, E.; Bangert, U.; Young, R. J. *2D Mater.* **2017**, *4* (1), 015007.
- (50) Alexeev, E. M.; Catanzaro, A.; Skrypka, O.; Nayak, P.; Ahn, S.; Pak, S.; Lee, J.; Sohn, J.; Novoselov, K. S.; Shin, H.; Tartakovskii, A. I. *Nano Lett.* **2017**, DOI: 10.1021/acs.nanolett.7b01763.
- (51) Carvalho, B. R.; Malard, L. M.; Alves, J. M.; Fantini, C.; Pimenta, M. A. *Phys. Rev. Lett.* **2015**, *114* (13), 136403.
- (52) Gaur, A. P. S.; Sahoo, S.; Scott, J. F.; Katiyar, R. S. *J. Phys. Chem. C* **2015**, *119* (9), 5146–5151.